Application of Laser-induced Thermal Emission in Imaging of Rough Surface Relief

Kateryna Zelenska[1,*], Olga Tkach[2], Serge Zelensky[2], Olexandr Kolesnik[2] and Toru Aoki[1]

[1] *Research Institute of Electronics, Shizuoka University, Hamamatsu, 432-8011, Japan*

[2] *Faculty of Physics, Taras Shevchenko National University of Kyiv, City of Kyiv, 01033, Ukraine*

Received: 2 June 2021, Revised: 28 June 2021, Accepted:28 June 2021

Abstract

For visualization of the microstructure of rough surfaces, a technique based on laser-induced heating of subsurface layers and observation of accompanying thermal emission is proposed. Transient temperature fields in the subsurface layers of a rough carbon surface and its time-integrated radiant exitance were calculated. A roughness element on a surface was given as a submicrometer-sized truncated-cone-shaped hole and peak. Computer simulations showed that local radiant exitance tenfold varied along the surface. This was due to (1) limited heat distribution at the peak tops and (2) enhanced heat outflow into the subsurface layer at the foot of a roughness hill (i) as well as at the bottom of the cavity in the vicinity of its walls (ii). In experiments, variations in the local radiant exitance on a rough carbon surface under pulse laser excitation were confirmed. The obtained photo images of rough carbon surfaces under laser irradiation were revealed to be high-contrast and suitable for the estimation of surface roughness employing a common optical microscope.

Keywords: Laser-induced thermal emission, Laser-induced incandescence, Radiant exitance map, Nanosecond laser pulses, Rough surface, Carbon.

1. Introduction

Nowadays, a huge diversity of methods for surface relief visualization is available: from direct visual observation to special indirect fine microscopy. But direct optical methods cannot provide appropriate image detail and contrast in the case of the surfaces with roughness size of submicrometer orders. At the same time, fine microscopy is cost and requires special sample preparation, measurement environment, etc. The main goal of research represented in this paper is to find an optimal decision for monitoring of roughness of a surface subjected to laser polishing and treatment employing IR nanosecond laser pulses.

When light-absorbing material is irradiated with a nanosecond laser pulse of moderate energy density, laser-induced thermal emission (LITE) is observed [1]-[7]. Another term used for such kind of emission and well-known in literature is laser-induced incandescence (LII) [8-20]. This phenomenon is occurred due to laser-induced heating of the samples up to a temperature of a few thousands of Kelvin. As a result, the overheated object turns into an emitter of pulse thermal radiation. The optical spectrum of the emission lies in the visible range of electromagnetic radiation and can be approximated by the Plank function for a black-body emission with good accuracy. The temperature of laser-heated objects such as carbon microparticles [7] and surfaces [17], [19] was estimated by calculations and from the experimental data. Moreover, the temperature of a light-absorbing surface under laser processing can be estimated employing a single-wavelength measurement of LII [17].

As known, LII was studied in (1) carbon microparticle suspensions in gases [8]-[11], liquids [7], [11], polymers [4], [13], some solids [5], and in (2) light-absorbing surface layers [6], [14]-[20]. The parameters of LII of carbon microparticles suspended in flames and exhaust

Corresponding Author : czelenska@gmail.com

gases, water (carbon black suspensions), or polymers such as gelatin, epoxy resin, polystyrene strongly depend on the particle size and can find its application for size estimation of soot particles, engine monitoring, control and monitoring of laser-induced marking in polymers, etc.

The techniques based on thermal emission observation are promising for diagnostics of surface roughness and temperature under laser processing [15], [17], visualization of microinclusions in the subsurface region [18], and porosity of porous carbons [14], as well as can be used to distinguish variations of such environment parameter as air pressure [16]. Moreover, studies of thermal emission can be used in the development of special methods known as laser-induced thermal emission spectroscopy [1]-[3].

In this work, we propose a technique for surface relief visualization based on observation of laser-induced thermal emission of a rough carbon surface via an optical microscope. This technique is based on inhomogeneous temperature distribution in protrusions on a surface under local laser-induced heating.

2. Experimental details

2.1 Calculations

The computer modeling was carried out with a single roughness element irradiated by a laser pulse propagating along the axis z. The model was also described in previous works [6,14,15]. The surface roughness was simulated by a truncated-cone protuberance (Fig. 1) or hole (Fig. 2) on the cylindrical basement. In Figs. 1 and 2, H = 7 μm, R = 5 μm are basement height and radius respectively, h is the height of the protuberance or the depth of the hole, r_1 and r_2 are radii of the upper and lower bases of the truncated cone. In the performed calculations, the dimensions comply with the following conditions: $r_1 = h$, $r_2 = 1.1r_1$ for protuberances and $r_1 = 2h$, $r_2 = 1.1r_1$ for holes.

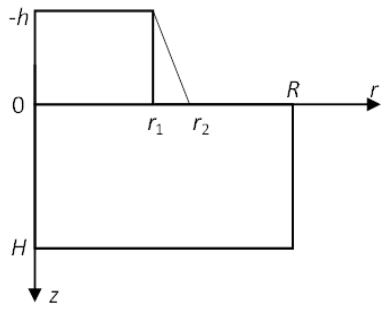

Fig. 1. Roughness element of a protuberance form

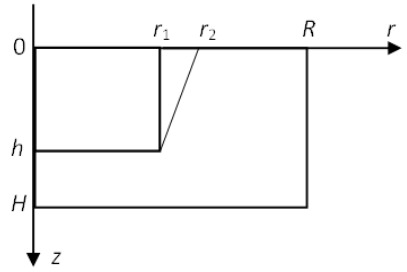

Fig. 2. Roughness element of a hole form

For laser-induced heating of surface roughness, the absorption of laser radiation is described by the following equation:

$$dF = -\alpha F dz \tag{1}$$

where F is the surface power density of laser radiation, α is the absorption coefficient at the laser wavelength λ = 1,064 nm. The laser pulse shape was presented in a rectangular form with the height F_0 and the pulse duration τ = 20 ns.

In the calculation, the heat conduction equation is represented in the following form:

$$c_p \frac{\partial T}{\partial t} = \nabla(\varkappa \nabla T) + \alpha F \tag{2}$$

where c_p is heat capacity, $\varkappa$ is thermal conductivity. It is supposed that the coefficients of heat capacity and thermal conductivity are independent of temperature and laser radiation intensity. The penetration depth of laser radiation into the material is determined as $\Delta = \frac{1}{\alpha}$, and the length of thermal diffusion – $\delta = \sqrt{\frac{\varkappa \tau}{c_p}}$. To minimize the whole sample heating, the dimensions H and R are chosen to exceed the parameters δ and Δ.

The solution of equations (1) and (2) is the transient distribution of surface temperature $T(r,t)$. Obtained surface temperature allows to calculate of radiant exitance $\varepsilon(r,t)$ using the Planck formula for a black body emission:

$$\varepsilon(r,t) = \frac{4\pi^2 \hbar c^2}{\lambda^5} \frac{\Delta\lambda}{exp\left(\frac{2\pi\hbar c}{\lambda k_B T(r,t)}\right) - 1} \tag{3}$$

where $\hbar$ is Planck's constant, c is the speed of light, k_B is Boltzmann's constant. It is supposed that thermal emission is detected within a narrow spectral interval $(\lambda,\ \lambda + \Delta\lambda)$. For the calculations, λ = 450 nm was chosen.

Under the irradiation of a sample by a single nanosecond laser pulse, its thermal emission is typically a sub-microsecond-timescale pulse with a short leading edge and a diminishing tail. The time-integrated radiant exitance E(r) is calculated as follows:

$$E(r) = \int \varepsilon(r,t) dt \tag{4}$$

2.2 Preparation of TiO_2/MB nanocomposite layer by a screen printing technique

For laser-induced thermal emission excitation, a Q-switched YAG:Nd laser was used (pulse duration τ = 20 ns, wavelength λ = 1,064 nm). The images of surfaces were made with an Olympus C-765UZ camera through a microscope with LOMO-8-0.20 object lens and K15x eyepiece lens. The snapshots with laser-induced thermal emission were made in a single-shot laser regime, without accumulation.

Carbon samples with rough surfaces were prepared similarly to [15]. Pharmaceutical activated carbon pellets and oak charcoal samples were used. SEM images of the sample surfaces are given in [15].

As is concluded in [15], the thermal conductivity of rough surface layers of carbon materials can be estimated as 0.08 W/m K. This estimate is significantly less than the values typically accepted in the literature for bulk carbon materials. Hence, the estimate of temperature diffusion length is as small as several dozens of nanometers. As far as the estimation of δ is relatively small, the expected spatial scale of local variations of the

luminosity of carbon surface layers is beyond the spatial resolution of typical optical microscopes, and the experimental setup will give a blurry picture of the luminosity variations.

3. Results and discussion

The calculated greyscale maps of time-integrated radiant exitance E (expression (4)) for different combinations of material parameters ($\Delta/\delta = 5$ in Fig. 3 and ($\Delta/\delta = 0.5$ in Fig. 4) and for various peak and hole sizes are given in Figs. 3 and 4. Left columns in Figs. 3 and 4 represent integrated radiant exitance data for surface elements of a truncated cone shape, and right columns - for elements with holes, where x, y coordinates along the surface (corresponding to $z = 0$).

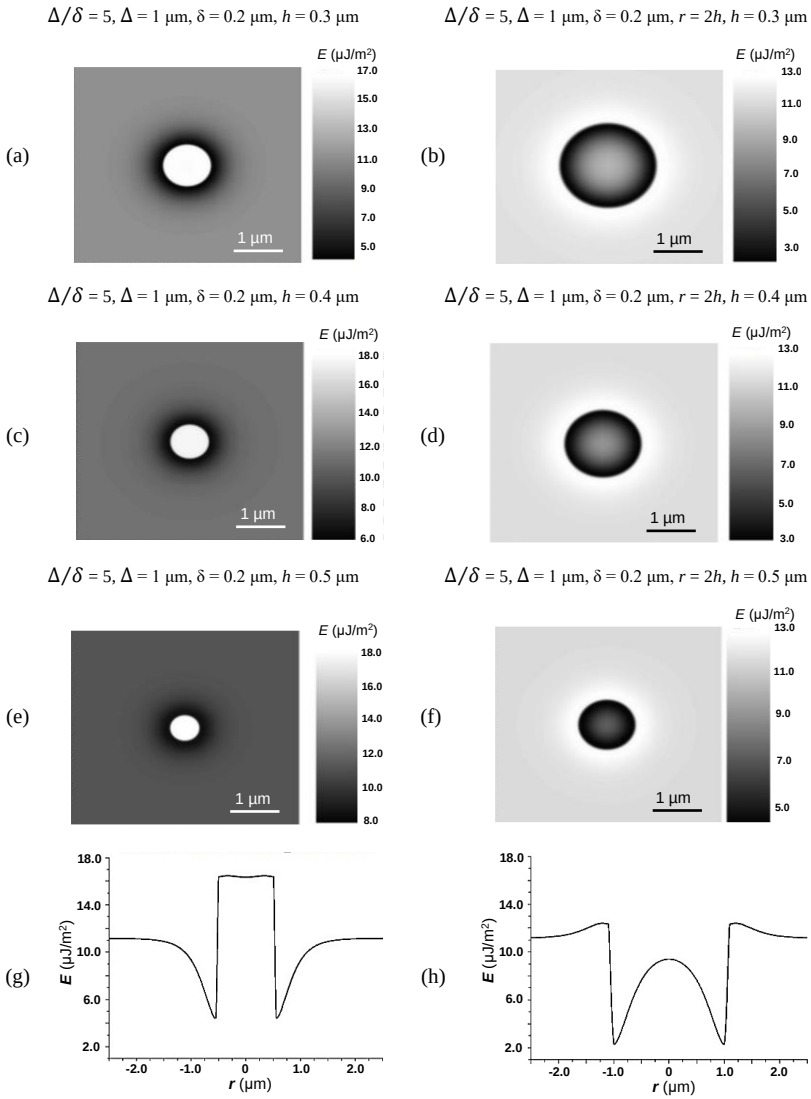

Fig. 3. Greyscale maps (a)-(f) and plots (g), (h) of time-integrated radiant exitance for $\Delta/\delta = 5$ ($\Delta = 1\mu m$, $\delta = 0.2\mu m$) and for different sizes of peaks (a), (c), (e), (g) and holes (b), (d), (f), (h): $h = 0.3$ μm (a), (b), 0.4 μm (c), (d), 0.5 μm (e)-(h)

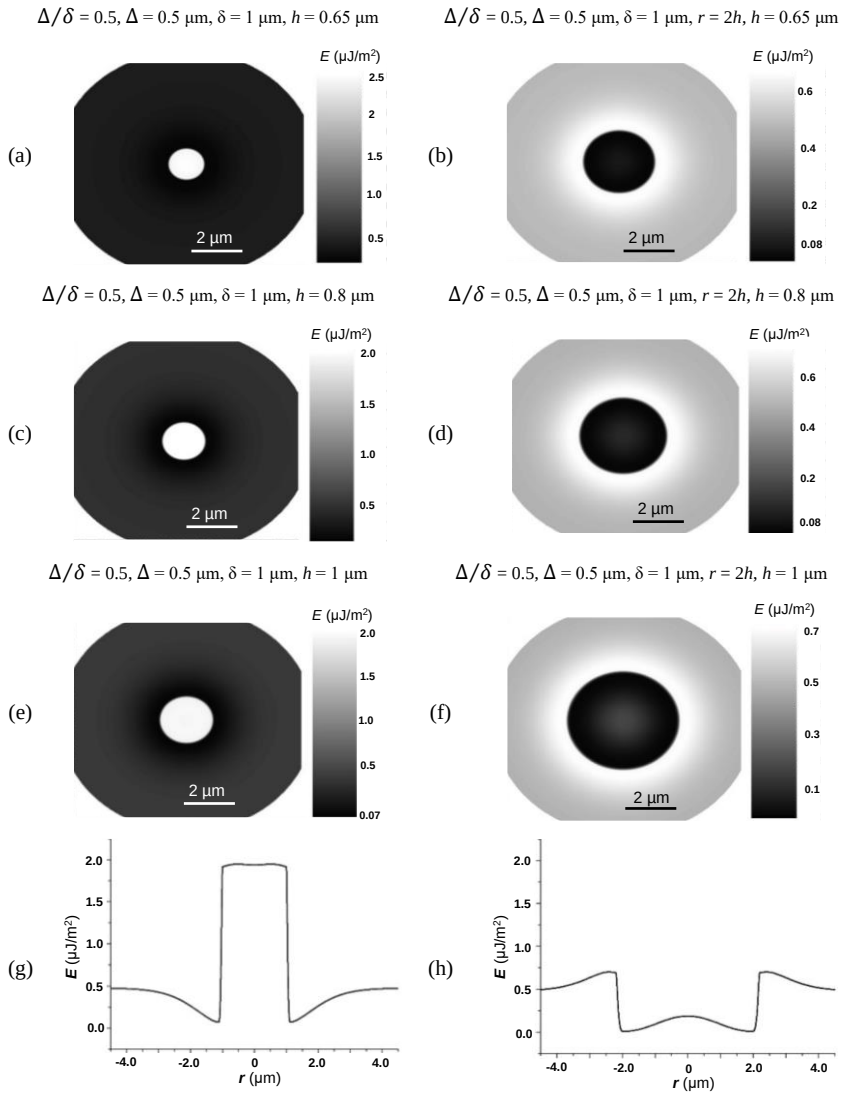

Fig. 4. Greyscale maps (a)-(f) and plots (g), (h) of time-integrated radiant exitance E for $\Delta/\delta = 0.5$ ($\Delta = 0.5$ μm, $\delta = 1$ μm) and for different sizes of peaks (a), (c), (e), (g) and holes (b), (d), (f), (h): $h = 0.65$ μm (a), (b), 0.8 μm (c), (d), 1 μm (e)-(h)

In all of the calculations, the intensity F_0 of laser radiation was adjusted to obtain the maximal laser-induced temperature $T_{max} \approx 3{,}000$ K on a flat area of a sample surface. This corresponds to the edges of surface elements ($z = 0$, $r = R$). However, the time-integrated radiant exitance E depends not only on T_{max} but also on the kinetics of temperature $T(t)$ and exitance $\varepsilon(t)$. That is why the time-integrated radiant exitance E at the edges of surface elements is different for different combinations of material parameters ($E = 11$ μJ/m^2 for $\Delta/\delta = 5$, Fig. 3 and $E = 0.5$ μJ/m^2 for $\Delta/\delta = 0.5$, Fig. 4).

First, consider the case when the laser-induced temperature wave does not leave the volume in which heat is generated during the laser pulse (see Fig. 3). This case is implemented at the ratio of parameters $\Delta/\delta > 1$. In this case, the following parameters were chosen for

calculations: $\varkappa$ = 2 W/m K, c_p = 10^6 J/m^{3}K, α = 10^6 m^{-1}, at which Δ/δ = 5. Greyscale maps of radiant exitance E for surface elements with cone peaks of increasing height 0.3 μm, 0.4 μ m, and 0.5 μm are presented in Fig. 3(a), (c), and (e). Similar maps for surface elements with holes of the same depth are shown in Fig. 3(b), (d), and (f). The sizes of peaks and holes depicted in Fig. 3 are chosen to be of the order of the value of thermal diffusion length = δ 0.2μ m. As a result, the surface distribution of time-integrated radiant exitance, E demonstrated important peculiarities presented in Fig. 3(g) and (h).

As seen from Fig. 3(g), the time-integrated radiant exitance E of the top surface of the cone peak exceeds the exitance of the flat surface by approximately 50%, hence the cone peak looks like a white circle on a grey surface. Besides, the time-integrated radiant exitance E has a significant decrease in the region around the cone peak (about 2.7 times smaller as compared with a flat surface), and this decrease is clearly visible on the greyscale maps presented in Fig. 3(a), (c), and (e) as a dark rim around the white circle.

For truncated-cone-shaped holes, as is seen from Fig. 3(h), the time-integrated radiant exitance E also has a decrease on the edge of the bottom surface of the hole; hence, the holes are visible as dark circles with the lighter central region. With the increase of hole radius, the exitance E of its center tends to the appropriate value of a flat surface.

Now consider the case when the laser-induced temperature wave has enough time to leave the volume of heat generation (see Fig. 4). In this case, tFige following relation holds < 1, and the material's parameters for calculations were chosen as follows: $\varkappa$ = 50 W/m K, c_p= 10^6 J/m^{3}K, α = $2\cdot10^6$ m^{-1}, Δ/δ = 0.5. For truncated-cone peaks, as is seen from the plot in Fig. 4(g), the time-integrated radiant exitance of the top surface of the peak (2.5 μJ/m^2) is five times larger than the exitance of a flat surface (0.5 μJ/m^2); hence, peaks can be visible as bright circles on the surface. It should be noted, in this case (= 0.5), the increase of exitance of peaks is much larger than in case = 5. Besides, in the regions around the peaks, the time-integrated radiant exitance E is also decreased significantly (in 7 times in Fig. 4(g)) as compared with the flat surface.

Concerning truncated-cone-shaped holes with = 0.5, the decrease of the exitance E at the edge of the bottom surface of the hole is also observed (see Fig. 4(h)), similarly to the case = 5.

The above-presented results of calculations give grounds to conclude, that the presence of a peak or a hole on the laser-irradiated surface leads to significant variations of local temperature and time-integrated radiant exitance. The exitance demonstrates local increases and decreases, with the appropriate maximal and minimal values given in Table 1. As is seen from Table 1, variations of local time-integrated radiant exitance E is more pronounced in materials with $\Delta < \delta$.

Table 1. Local time-integrated radiant exitance E for peaks and holes according to Figs. 3, 4 - (g), (h)

***E*, μJ/m^2**	**Δ/δ = 5 peak**	**Δ/δ = 5 hole**	**Δ/δ = 0.5 peak**	**Δ/δ = 0.5 hole**
Maximal	17	13	2.5	0.7
Minimal	4	2	0.07	0.02
Flat surface	11	11	0.5	0.5
E_{max} / E_{min}	4.25	6.5	35	35

As is shown in [18], laser-induced thermal emission can be useful for the visualization of hidden undersurface inhomogeneities of thermal and optical characteristics of the irradiated material. The above-presented results of computer modeling also show that laser-induced thermal emission can be useful for the visualization of the roughness of light-absorbing materials. Figs. 3 and 4 demonstrate a possibility not only to reveal the presence of a microscopic peak or hole on a laser-irradiated surface but also to distinguish peaks and holes by their visual appearance in thermal emission.

It should be noted, that calculations considered above were performed with hypothetical sets of material parameters that corresponded to the cases $\Delta/\delta = 5$ and $\Delta/\delta = 0.5$. For practical realization of pulsed laser heating of rough surfaces, possibilities of choosing the materials with the necessary sets of parameters are strongly limited. Typical materials which demonstrate clearly visible laser-induced thermal emission are carbonaceous materials [4], [12], [14], [15]. Thermal characteristics of carbon in various modifications are comprehensively reviewed in [21]. Thermal conductivity demonstrates significant variations in different carbon materials [21]. Besides, thermal characteristics of carbon are temperature-dependent [21]-[23], and this dependence is not well known in the temperature interval 2,000-4,000 K where the laser-induced thermal emission can be easily detected.

It also should be noted, that thermal diffusivity of carbon forming rough surface layers can differ significantly from the characteristics of bulk carbon as is shown in [15]. As is predicted in [6], [15], based on the investigations of kinetics of laser-induced thermal emission, rough carbon surface layers can be attributed to case $\Delta/\delta \approx 7$. Therefore, for rough surface layers of carbon materials, we can expect that laser-induced thermal emission will demonstrate variations of local time-integrated radiant exitance that are presented in Table 1.

A typical example of the surface scan of the time-integrated radiant exitance of activated carbon pellet is given in Fig. 5, where x is a coordinate along a surface.

Corresponding images of the same fragments of oak charcoal surface illuminated by an incandescent lamp (a), (c), (e) and irradiated by a powerful laser pulse (b), (d), (f) are represented in Fig. 6. As the camera was non-sensitive to the laser IR radiation, images “(b)”, “(d)”, and “(f)” were formed by laser-induced thermal emission of the irradiated surface. As is seen from the figure, the layered structure of the sample is visible in all pairs of images. It should be noted that images (a), (c), (e) and (b), (d), (f) do not coincide, and laser-induced thermal emission reveals some surface features invisible under the lamp illumination.

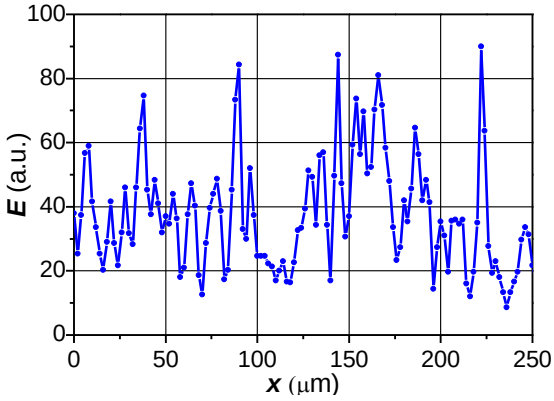

Fig. 5. Typical time-integrated radiant exitance E as a function of coordinate along the surface of activated carbon pellet

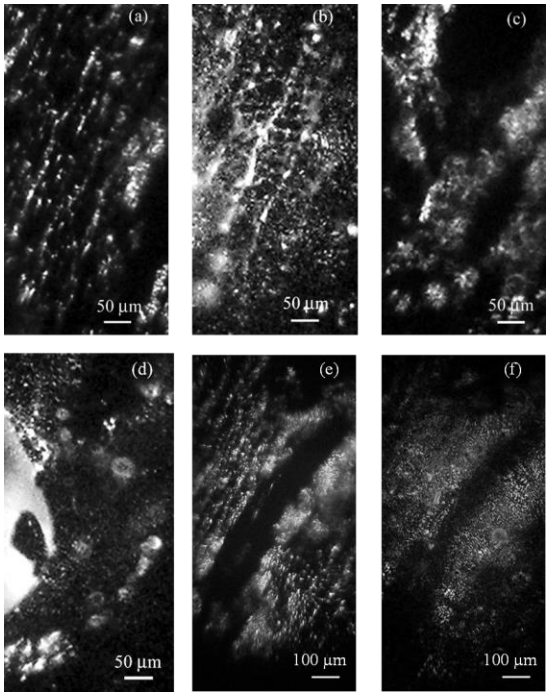

Fig. 6. Typical images of oak charcoal samples illuminated by the lamp (a), (c), (e) and by YAG:Nd laser (b), (d), (f)

As can be concluded from the calculation results (Figs. 3 and 4), dimensions of the regions, where variation of the local radiant exitance reached pronounced difference, were in orders of a micrometer that was beyond the capabilities of the used equipment. Thus, dependence of time-integrated radiant exitance on the coordinate along the surface presented in Fig. 5 was used to estimate only the ratio of local maximal and minimal values. The exitance demonstrates significant variations with the ratio of local maximal and minimal values of the order of $E_{max} / E_{min} \sim 5$. The obtained ratio was of the same order of magnitude as obtained from the calculations for $\Delta/\delta = 5$ (Table 1).

4. Conclusion

Laser-induced thermal emission is a kind of secondary emission that is sensitive to the structure of the irradiated surface layer. It was revealed that the local exitance of laser-induced thermal emission and its kinetics depends on the shape and size of the elements forming the surface roughness relief. Besides, the characteristics of laser-induced thermal emission are also sensitive to the variations of local thermal and optical parameters of the material forming the surface layer at a depth of the order of the laser penetration depth Δ and the temperature diffusion depth δ. Laser-induced thermal emission can be used in studies of properties of light-absorbing materials and for visualization of the surface structure and relief.

Acknowledgement

This research was partly supported by 2020 Cooperative Research at Research Center of Biomedical Engineering, Japan, adopted as 2020 Cooperative Research at RIE, Shizuoka University (Grant No. 2065), 2021 Cooperative Research at Research Center of Biomedical

Engineering, Japan, adopted as 2021 Cooperative Research at RIE, Shizuoka University (Grant No. 2067), and by Taras Shevchenko National University of Kyiv (Project No. 19BF051-02).

References

[1] Galán-Freyle NJ, Pacheco-Londono LC, Figueroa-Navedo AM, Hernandez-Rivera SP. Standoff detection of highly energetic materials using laser-induced thermal excitation of infrared emission. Appl. Spectrosc. Rev. 2015;69(5):535-44.
[2] Lin LT, Archibald DD, Honigs DE. Preliminary studies of laser-induced thermal emission spectroscopy of condensed phases. Appl. Spectrosc. Rev. 1988;42(3): 477-83.
[3] Tsuge A, Uwamino Y, Ishizuka T. Applications of laser-induced thermal emission spectroscopy to various samples. Appl. Spectrosc. Rev. 1989;43(7):1145-9.
[4] Zelensky S, Kolesnik A, Kopyshinsky A, Garashchenko V, Zelenska K, Stadnytsky V, Shinkarenko E. Thermal emission of carbon microparticles in polymer matrixes under pulsed laser excitation. Ukr. J. Phys. 2009;54(10):983-8.
[5] S. Zelensky, Laser-induced heat radiation in borate glass. J. Phys.: Condens. Matter 1998;10(32):7267-72.
[6] Zelensky S, Aoki T. Decay kinetics of thermal emission of surface layers of carbon materials under pulsed laser excitation, Opt. Spectrosc. 2019;127:931-7.
[7] Zelensky S. Laser-induced heat radiation of suspended particles: a method for temperature estimation. J. Opt. A: Pure Appl. Opt. 1999;1 :454-8.
[8] Hofmann M, Bessler WG, Schulz C, Jander H. Laser-induced incandescence for soot diagnostics at high pressures. Appl. Opt. 2003;42(12):2052-62.
[9] Michelsen HA. Laser-induced incandescence of flame-generated soot on a picosecond time scale, Appl. Phys. B 2006;83(3):443-8.
[10] Vander Wal RL, Ticich TM, Stephens A. Can soot primary particle size be determined using laser-induced incandescence? Combust. Flame 1999;116:291-6.
[11] Michelsen HA, Schulz C, Smallwood GJ, Will S. Laser-induced incandescence: Particulate diagnostics for combustion, atmospheric, and industrial applications. Prog. Energy Combust. Sci. 2015;51:2-48.
[12] Rulik JJ, Mikhailenko NM, Zelensky SE, Kolesnik AS. Laser-induced incandescence in aqueous carbon black suspensions: the role of particle vaporization. Semicond. Phys. Quantum Electron. Optoelectron. 2007;10(2):6-10.
[13] Zelenska KS, Zelensky SE, Poperenko LV, Kanev K, Mizeikis V, Gnatyuk VA. Thermal mechanisms of laser marking in transparent polymers with light-absorbing microparticles. Opt. Laser Technol. 2016;76:96-100.
[14] Karpovych V, Zelenska K, Yablochkov S, Zelensky S, Aoki T. Evolution of laser-induced incandescence of porous carbon materials under irradiation by a sequence of laser pulses. Thai J. Nanosci. Nanotechnol. 2017;2(2):14-20.
[15] Karpovych V, Tkach O, Zelenska K, Zelensky S, Aoki T. Laser-induced thermal emission of rough carbon surfaces. J. Laser Appl. 2020;32(1):012010.
[16] Zelenska KS, Kopyshinsky AV, Poperenko LV. Laser-induced incandescence of carbon surface at various values of ambient air pressure. Proc. IEEE, Fotonica AEIT Italian Conference on Photonics Technologies;2014 May 12-14; Naples Italy. Napoli: 2014. p.1-3.
[17] Zelensky S, Zelenska K. Laser-induced incandescence of carbon surface: a method for temperature estimation, Proc. SPIE Int. Soc. Opt. Eng. 2013;8772:1-8.
[18] Kokhan M, Koleshnia I, Zelensky S, Aoki T. On the possibility of visualization of undersurface submicron-sized inhomogeneities via laser-induced incandescence of

surface layers. Proc. High-Power Laser Materials Processing: Applications, Diagnostics, and Systems VI. 2017;100970:1-7.
[19] Zelensky S, Poperenko L, Kopyshinsky A, Zelenska K. Nonlinear characteristics of laser-induced incandescence of rough carbon surfaces. Proc. Nonlinear Optics and Applications VI. 2012;84341:1-6.
[20] Kopyshinsky AV, Zelensky SE, Gomon EA, Rozouvan SG, Kolesnik AS. Laser-induced incandescence of silicon surface under 1064-nm excitation. Semicond. Phys. Quantum Electron. Optoelectron. 2012;15(4):376-81.
[21] Ho CY, Powell RW, Liley PE. Thermal conductivity of the elements: A comprehensive review. J. Phys. Chem. Ref. Data 1974;3:1–756.
[22] Butland ATD, Maddison RJ. The specific heat of graphite: An evaluation of measurements. J. Nucl. Mater. 1973;49:45-56.
[23] McDonald RA. Heat content and heat capacity of an extruded graphite from 341° to 1723°K. J. Chem. Eng. Data 1965;10:243.